Journal of Information Systems Engineering and Management
2026, 11(3s)
e-ISSN: 2468-4376
https://www.jisem-journal.com/

Research Article

Influence of Physical Parameters on p-CuO/n-CdS/n-Zn_2SnO_4 Solar cell: A Numerical Investigation Achieving Efficiency of 28.50 % Using SCAPS-1D

Mouad Chettab [1]*, Halima Djaaboube [1], Safia Harrat [2], Sihem Abed [3], Yassine Bouachiba [4], Redha Aouati [1], Adel Taabouche [3], Ouassila Benzaoui [1], Abderrahmane Bouabellou1[1]

[1] *Laboratoire Couches Minces et Interfaces, Université des Frères Mentouri Constantine 1, Constantine, Algérie.*
[2] *Université des Frères Mentouri Constantine 1, Constantine, Algérie.*
[3] *Département de Physique et Chimie, Ecole Normale Supérieure El Katiba Assia Djebar Constantine, Constantine, Algérie.*
[4] *Laboratoire Technologie des Matériaux Avancés, Ecole Nationale Polytechnique de Constantine Malek Bennabi, BP 75A RP, Ali Mendjeli, Constantine, Algérie.*
* Corresponding Author: chettabmouad96@gmail.com

ARTICLE INFO

Received: 28 Dec 2024
Revised: 18 Feb 2025
Accepted: 26 Feb 2025

ABSTRACT

This work presents a comprehensive numerical investigation of CuO thin-film solar cells using SCAPS-1D, focusing on replacing conventional CdTe and CIGS absorber layers with environmentally friendly alternative CuO metal oxide. The simulation explores the influence of absorber, buffer and window layer thicknesses, as well as temperature on the key photovoltaic parameters of CuO-based devices. The optimization study shows that an absorber thickness of 4 µm maximizes light absorption without excessive recombination, while the buffer and window layers achieve optimal performance at 0.02 µm. The results indicate that increasing the temperature from 300 K to 400 K causes a gradual decline in efficiency from 21.62 % to 16.58 %. Furthermore, specific parameters of p-CuO/n-CdS/n-Zn_2SnO_4 heterostructure, such as the influence of defects density, acceptor concentration, metal work function, Rs and Rsh were examined. Our findings revealed that the efficiency could be improved by increasing the acceptor concentration of p-type CuO layer and metal work function of the contact and reduced defects density and balancing between R_s and R_{sh}. The optimized p-CuO/n-CdS/n-Zn_2SnO_4 configuration attains a high conversion efficiency of 28.50 % under AM 1.5 illumination, demonstrating that CuO solar cell can achieve competitive performance. This study provides valuable insights for the design of cost-effective, non-toxic, and high-efficiency photovoltaic devices.

Keywords: SCAPS-1D, Thin films, Solar cells, CuO, CdS, Zn_2SnO_4, Efficiency.

INTRODUCTION

The increasing global demand for energy has become a significant challenge, especially as traditional energy sources are no longer sufficient to meet growing needs [1, 2]. Renewable energy has emerged as a viable solution [3] for the future and photovoltaic energy source is attracting great attention and employed in several domains [4, 5]. But it still faces some obstacles related to efficiency and production costs, particularly with recent advancements that have improved their efficiency and productivity [6]. However, the cost of materials used in manufacturing these panels remains a barrier to widespread adoption. Therefore, the type of materials used plays a crucial role. In this context, metal oxides have really caught the attention of researchers in recent years, mostly because they can serve many different purposes in optoelectronic devices. Among them, copper-based oxides stand out the most candidate [4]. Material like cupric oxide CuO, cuprous oxide Cu_2O have been studied frequently because they are stable, easy to make, and full of interesting properties. They are both p-type materials, which means they naturally fit into thin-film solar cells as absorber layers. CuO has a monoclinic crystal structure [7] and a band gap usually between 1.0 and 2.1 eV [4]. One of the reasons it is cheap, non-toxic, and does not require complicated preparation [8]. It also has both direct and indirect band gaps, which helps its performance in solar devices. Cu_2O behaves differently. It has a

Journal of Information Systems Engineering and Management
2026, 11(3s)
e-ISSN: 2468-4376
https://www.jisem-journal.com/

Research Article

cubic structure [7] and a wider band gap somewhere around 2.0 to 2.6 eV [9]. That larger band gap makes it more transparent to visible light, giving it a different role and unique possibilities in optoelectronics. As result, copper oxide CuO is a promising absorber layer in thin-film solar cells due to its narrowband gap [1], high absorption coefficient (>105 cm-1) [10], and earth-abundant [11]. Its compatibility with heterojunction structures makes it a viable alternative to conventional CdTe and Cu(In,Ga)Se_2 absorbers [12]. However, optimizing its performance requires an appropriate window and buffer layer combination to enhance charges separation and reduce recombination losses.

The buffer layer plays a crucial role in adjusting band alignment, reducing interfacial defects, and improving overall device efficiency. Conventionally, cadmium sulfide CdS is widely used due to its high absorption coefficient, appropriate bandgap [13], excellent carrier mobility and strong electrical conductivity, allowing it to form an effective interface with the absorber layer and facilitate efficient charge transport [14]. It presents a facility in lattice match with CuO, leading to passivity interface defects. Additionally, Zn_2SnO_4, with its high optical transparency, wide bandgap (~3.0-3.2 eV) and excellent electron mobility [15-17]. These advantages allow to facilitate electron transport and minimizing parasitic absorption [18]. By selecting appropriate layers, the efficiency and stability of CuO-based solar cells can be improved.

Further research is needed to optimize the material deposition techniques and band alignment for enhanced performances. Sawicka-Chudy et al. [15] simulated n-TiO_2/p-CuO and n-TiO_2/p-Cu_2O heterojunction solar cells, present an analysis of layer thickness and defect density in buffer and absorber thin films that affect cell performance. They carried out a numerical study of J-V curves for n-TiO_2/p-Cu_2O solar cells and confirmed the potential of use of its structure based on the numerical simulations. Abdelfatah et al. [1] they achieved a power conversion efficiency (PCE) of 23.8% as the highest value for their simulated devices with the Voc value of 0.96 V, Jsc value of 34.2 mA/cm^2, and the FF value of 72.2%. Such efficiency was obtained when the CuO band gap, thickness, and carrier concentration was 1.35 eV, 5.5 µm, and above 10^{18} cm^{-3}, respectively. For the ZrS_2, they found 1.4 eV, 1µm, and less than 10^{20} cm^{-3}, respectively. Nevertheless, best work configuration, optimal material properties, preferred and boundary work conditions for high cell performance are still the issues that should be addressed. Thus, the authors decided to continue the structure analysis for comprehensive result acquirement. The main objective of this work is to serve experimenters in order to save time and money needed for solar cells manufacturing [19].

OBJECTIVES

Our study was based on modeling and simulation of CuO solar cells p-CuO/n-CdS/n-Zn_2SnO_4 to figure out the suitable alternative of CdTe and CIGS. In addition, improving the performance of solar cell by varying the temperature and different thicknesses of absorber layer p-CuO, buffer layer n-CdS and window layer n- Zn_2SnO_4 Zn_2SnO_4 [7]. Also, the defect density, acceptor concentration, Rs and Rsh were investigated to determine the optimized values. The numerical calculation study of thin film CuO-based solar cell was evaluated using SCAPS-1D, in order to design and optimize the photovoltaic parameters (PCE, FF, Voc and Jsc) under standard illumination (AM 1.5G, 1000 watt/m^2).

METHODS

In this study, the mathematical framework involves solving three interconnected partial differential equations, namely Poisson's equation, the continuity equations, and the transport equation, which are presented in equations (Eq.) (1), (2), (3), (4) and (5) [20].

These equations play a crucial role accurately describing the behavior of charge carriers within the solar cell.

Poisson's equation establishes the relationship between the electric charge and the electric potential in a specific area of space, as expressed in Eq. (1) [21, 22].

$$\frac{\partial^2 \psi}{\partial x^2} = \frac{-\partial E}{\partial x} = \frac{\rho}{\epsilon_s} = \frac{-q}{\epsilon_s}\left(p - n + N_d^+ - N_a^- \pm N_{def}\right) \quad (1)$$

The electrostatic potentiality denoted as ψ, it is measured in volts (V). While E represents the electric field with unit of (V/m), ρ is the charge density (C/m^3), ϵs refers to the static relative permittivity, measured in (F/m), q is the elementary charge (C), n and p are the respective electron and hole densities (number of particles per cubic meter),

Journal of Information Systems Engineering and Management
2026, 11(3s)
e-ISSN: 2468-4376
https://www.jisem-journal.com/

Research Article

N_+^d presents the density of donors (number of donors per cubic meter), N_-^a presents the density of acceptors (number of acceptors per cubic meter), and Ndef is the defect density of both donors and acceptors (number of defects per cubic meter).

The carrier continuity equation given in Eq. (2) and (3) [21-24] is a partial differential equation that describes the variation in change carrier density (electrons and holes) within a semiconductor device. These equations establish the relationship between the rate of change of carrier density to the net flow of carriers into and out of a given volume of the semiconductor device. By solving these equations, it is possible to predict their electrical performance under different operating conditions.

$$-\frac{\partial J_p}{\partial x}+G-U_P(n,p)=0 \quad (2)$$

$$-\frac{\partial J_n}{\partial x}+G-U_n(n,p)=0 \quad (3)$$

In this context, Jp shows the hole current density (A/m²), Jn is the electron current density (A/m²), G corresponds to the carrier generation rate (s/m³), Up(n,p) signifies the recombination rate of holes (s/m³), and Un(n, p) signifies the recombination rate of electrons (s/m³).

The transport equation outlined in Eq. (4) and (5) of a solar cell is a partial differential equation that characterizes the behavior of charge carriers (electrons and holes) as they move through the device. It takes into account various physical mechanisms that affect the transport of charge carriers, such as diffusion, drift, and recombination [25]. These equations relate the spatial and temporal variations of the carrier density, drift velocity, and diffusion coefficient to the applied electric field, carrier concentration, and recombination rates in the device [21].

$$J_p = q\mu_p - qD_p\frac{\partial p}{\partial x} \quad (4)$$

$$J_n = q\mu_n - qD_n\frac{\partial p}{\partial x} \quad (5)$$

Here, J_p is the hole current density (A/m²), J_n is the electron current density (A/m²), q is the charge (C), μp and μn are the carrier motilities (m²/V.s), E is the electric field (V/m), Dp and Dn are the diffusion coefficients (m²/s), $\frac{\partial p}{\partial x}$ is the spatial gradient of the hole concentration and $\frac{\partial p}{\partial x}$ is the spatial gradient of the electron concentration.

This study determines the absorption coefficient using the new model, an updated version of the earlier SCAPS model (the conventional Tauc's law ($\sqrt{h\upsilon - Eg}$ law model). There is an explanation of the model in the following Eq. (6) [10].

$$\alpha(h\upsilon) = \left(\alpha_0 + \beta_0\frac{E_g}{h\upsilon}\right)\sqrt{\frac{h\upsilon}{E_g}-1} \quad (6)$$

α is the optical absorption constant (cm-1), Eg represents the bandgap (eV), and hν is the photon energy (eV), α0 and β0 are the model constants. The relation between the model constants and conventional model constants A and B is shown in Eq. (7.1) and. (7.2) [10].

$$\alpha_0 = A\sqrt{E_g} \quad (7.1)$$

$$\beta_0 = \frac{B}{\sqrt{E_g}} \quad (7.2)$$

The device structure of the proposed solar cell is represented in figure 01. The buffer layer (CdS) is coated on Zn_2SnO_4 layer and the absorber layer (CuO) is situated on the buffer layer. The various device parameters required for simulation of these materials are shown in Table 01. The initial thickness of absorber, buffer and window layers are kept at 0.4 μm, 0.04 μm and 0.03 μm, respectively. They will be changed for determine the optimum thickness of each layer. The continuity and coupled Poisson equations at interfaces and contacts for both the charge carriers with the suitable boundary conditions, are shown in figure 02. The energy band alignment and the VBO and CBO formed by the layers of our solar cell are shown in figure 02. The VBO and CBO have been calculated from the electron affinity

Journal of Information Systems Engineering and Management
2026, 11(3s)
e-ISSN: 2468-4376
https://www.jisem-journal.com/

Research Article

χ and band gap Eg of the material using the formula [26]. Figure 03 shows the different steps and instructions for running SCAPS-1D.

$$CBO = \chi_{CdS} - \chi_{CuO} \quad (7.3)$$

$$VBO = \chi_{CuO} - \chi_{Zn2SnO4} + Eg_{CuO} - Eg_{Zn2SnO4} \quad (7.4)$$

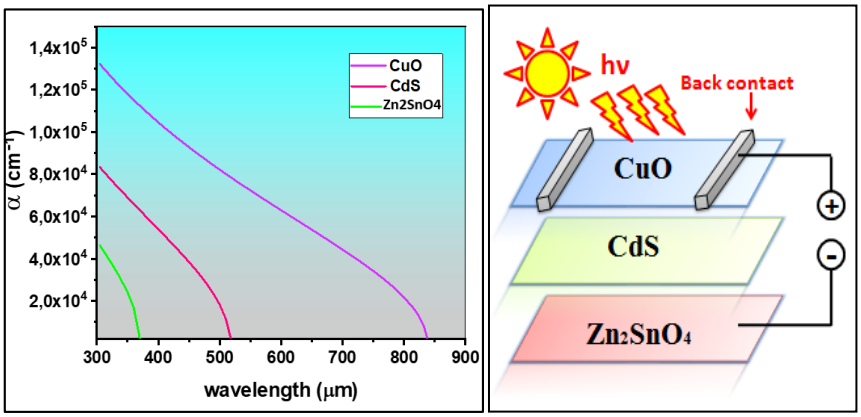

Figure 01. Variations of absorption coifficient (α) for each layer (left), solar cell desgin (right).

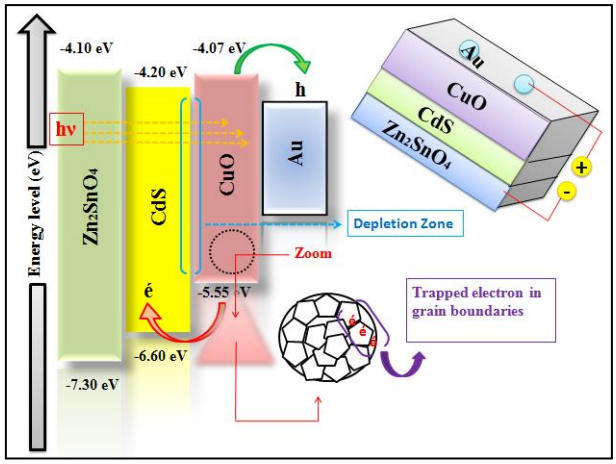

Figure 02. Variation energy levels in CuO based solar cell.

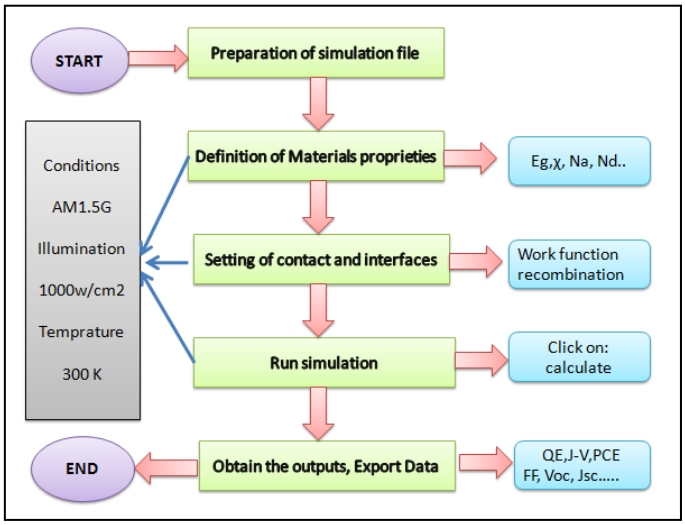

Figure 03. steps and instructions for running SCAPS-1D.

Journal of Information Systems Engineering and Management
2026, 11(3s)
e-ISSN: 2468-4376
https://www.jisem-journal.com/

Research Article

Table 01. Parameters for Zn_2SnO_4, CdS and CuO layers.

Parameter	Symbol	Unit	p-CuO	n-CdS	n-Zn_2SnO_4
Thickness	W	(µm)	02	0.04	0.04
Band gap	E_g	(eV)	1.48	2.4	3.35
Electron affinity	χ	(eV)	4.07	4.2	4.5
Dielectric permittivity	ε_r	(relative)	18.1	10	09
CB effective density of states	CB	(cm^{-1})	2.1E+19	1.5E+18	2.20E+18
VB effective density of states	VB	(cm^{-1})	5.5E+19	1.8E+19	1.80E+19
Electron thermal velocity	V_{th}	(cm/s)	1.0E+7	1.0E+7	1.0E+7
Hole thermal velocity	V_{th}	(cm/s)	1.0E+7	1.0E+7	1.0E+7
Electron mobility	μ_e	(m^2/V.s)	100	100	32
Hole mobility	μ_h	(m^2/V.s)	0.1	25	3
Shallow uniform donor density	N_d	(cm^{-3})	0	1.0E+15	1.0E+19
Shallow uniform donor density	N_a	(cm^{-3})	1.0E+15	0	0
Defects density	N_t	(cm^{-3})	1.0E+15	1.0E+15	1.0E+15
References	/	/	[10, 15]	[27]	[25]

RESULTS AND DISCUSSION

Temperature effect

In this part, the influence of operating temperature on the performance of solar cell p-CuO/n-CdS/n-Zn_2SnO_4 and its basic photovoltaic parameters were investigated and presented in figure 04. The decreasing in the open-circuit-voltage Voc with the increasing in temperature ranging from 300 K to 400 K can be explained by the reduction of semiconductors bandgap [28]. Since Voc depends on the differences in quasi-Fermi levels of electrons and holes which are influenced by band gap. The increasing in temperature leads to raise the recombination probability as result the Voc, the Jsc, and the PCE values reduced. The increasing in recombination probability and decline in photovoltaic parameters can be attributed to the decrease of the charge carrier distance, which raises recombination rates, and lowering the efficiency. Similar results were reported in [29]. In addition, the higher temperatures can provide the electrons more energy that is raises the mobility of the charges carriers and decreases their lifetime [30] and photocurrent generation. Moreover, the quantum efficiency QE was also investigated for different wavelengths ranging from 300 nm to 900 nm, as shown in figure 04. The optimal efficiency QE was 99% for 420 nm. As temperature increases, the quantum efficiency QE of solar cell generally exhibited a slight variation particularly in UV region as shown in zoomed section due to the reduction of the collected charges carriers' number and increased scattering by thermally activated phonons. Moreover, elevated temperature can activate more defects states at material interfaces, increasing carrier trapping further degrading the (J-V) characteristics [31].

The fitting curves in figure 04 confirmed a linear decay of PCE, FF, Voc and Jsc as the temperature increases. Determination of the temperature coefficient (C_T) applying the generalized linear relation becomes very much essential for a better understanding of the temperature performance correlation in real world condition as mentioned in the equations. Under standard test conditions (STC_ 300 K), the temperature coefficient $C_{T\text{-}Y}$ (Y= ŋ, FF, Jsc and

Journal of Information Systems Engineering and Management
2026, 11(3s)
e-ISSN: 2468-4376
https://www.jisem-journal.com/

Research Article

Voc) of photovoltaic parameters [16, 32]. Where, η_{STC} is the cell efficiency, FF_{STC} is the fill factor, Voc_{STC} is the open circuit voltage and Jsc_{STC} is the short circuit current density at STC.

$$C_{T-\eta} = \frac{1}{\eta_{STC}} \frac{d\eta}{dT} \times 100 \quad (8)$$

$$C_{T-FF} = \frac{1}{FF_{STC}} \frac{dFF}{dT} \times 100 \quad (9)$$

$$C_{T-Voc} = \frac{1}{Voc_{STC}} \frac{dVoc}{dT} \quad (10)$$

$$C_{T-Jsc} = \frac{1}{Jsc_{STC}} \frac{dJsc}{dT} \quad (11)$$

Simulation results indicate the thermal stabilization coefficients for the solar cell as follows: an efficiency drop of 0.27 $\%K^{-1}$, an open-circuit voltage decrease of 2.29 $mV.K^{-1}$, a fill factor reduction of 0.06 $\%.K^{-1}$. The efficiency drop suggests that for every 10 K temperature rise, the solar cell loses 0.55 % of its efficiency, which is relatively acceptable. The decrease in Voc needs further verification since typical values for CuO are around 2 to 3 $mV.K^{-1}$. The Jsc show minor changes with temperature, indicating they are less affected by thermal fluctuations. Overall, the cell exhibits moderate thermal stability, but its efficiency degradation suggests that its performance significantly declines at elevated temperatures. The solar cell would not suffer from severe voltage losses, making it suitable for high-temperature applications.

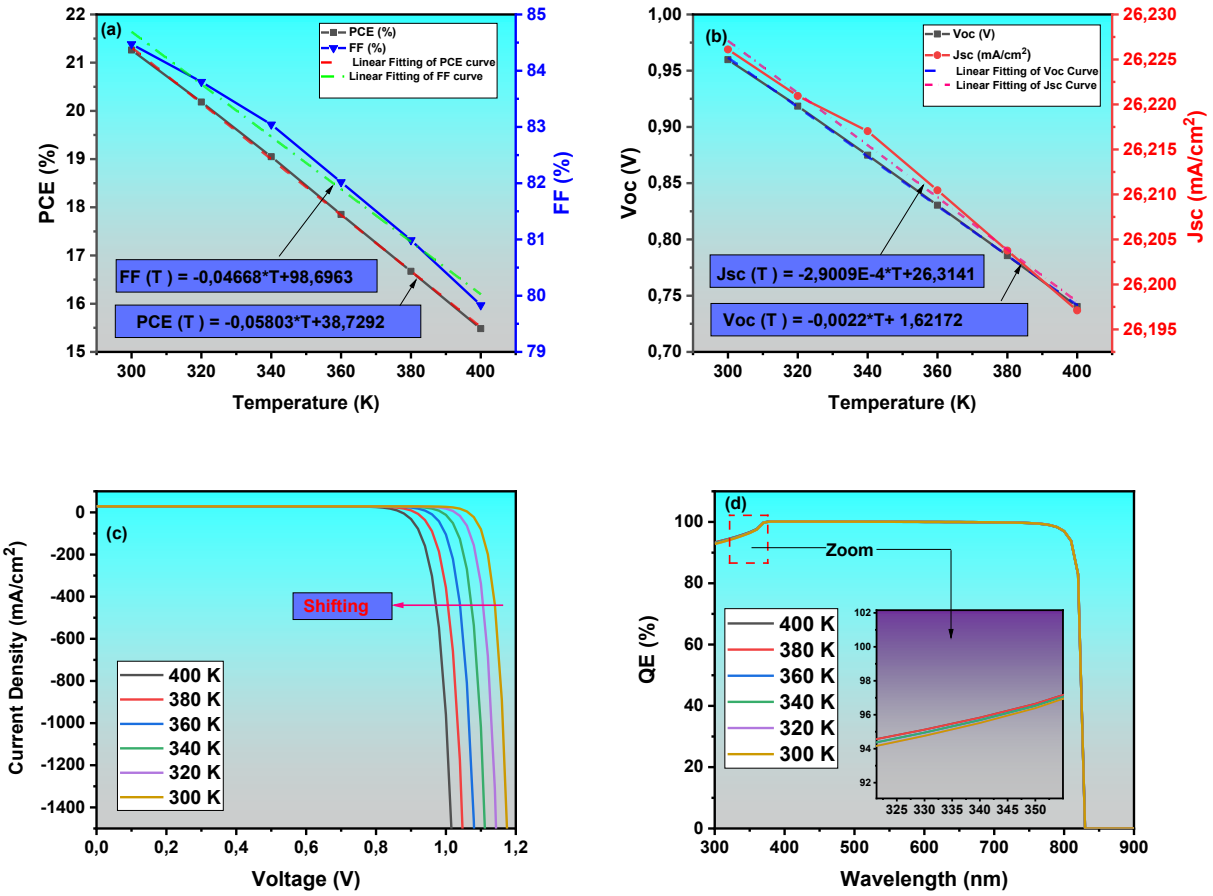

Figure 04. (a) and (b) Variations of Voc and Jsc, PCE and FF versus temperature. (c) and (d) variation of (J-V) and (QE) curves with increasing of temperature.

Journal of Information Systems Engineering and Management
2026, 11(3s)
e-ISSN: 2468-4376
https://www.jisem-journal.com/

Research Article

Thickness effect of absorber layer (CuO)

As the other semiconductor devices, the solar cell is sensitive to geometric parameters like thickness, which influences the photovoltaic parameters (Jsc, Voc, FF and PCE). In this work; the photovoltaic parameters have been calculated for different thickness of absorber layer CuO ranging from 1 µm to 6 µm. According to figure 05, it is clear that the PCE and FF increased to 24.01 % and 86.70 % at 5 µm followed by gradual stabilization at higher thickness indicating that the CuO layer has reached a sufficient thickness to absorb photons without significant additional gains. Also, the Voc and Jsc showed the same trend, Voc and Jsc increased to 0.98 V and 27.6 mA/cm² respectively at 5 µm. This behavior can be explained by several reasons. On one hand, the thicker layers of CuO, different wavelengths penetrate the solar cell at different depths, the absorber layer CuO increases the optical path length allowing photons to travel further [12], which is raises the probability of photon absorption and enhanced absorbed photons results a high generation of charge carriers, the generated pairs contribute to generated current and reduced the recombination [26, 33]. On other hand, the thinner layers, only the short wavelengths can penetrate the solar cell which is reduces the probability of photon absorption and the generated pairs. These electrons and holes generated near the back of absorber layer may not reach the solar cell and instead recombine [34]. Hossain et al. [35] reported the same observations. The QE spectrum and J-V characteristic curves exhibited a shifting with the increasing of thickness, which enhanced the collection and separation of pairs, and reflecting positively on photovoltaic parameters and confirming our findings.

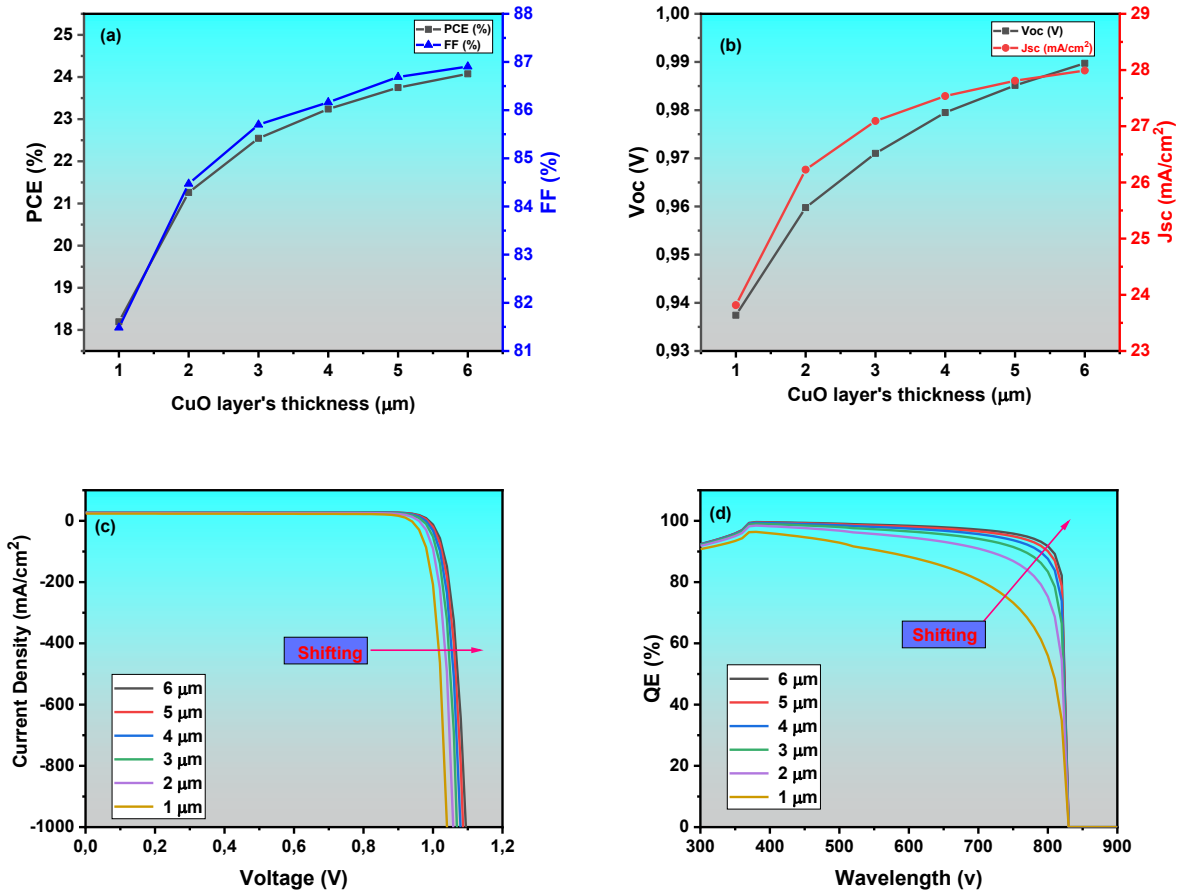

Figure 05. (a) and (b) Variations of Voc, Jsc , PCE and FF versus CuO's thickness. (c) and (d) variation of (J-V) and (QE) curves with increasing of thickness.

Thickness effect of buffer layer (CdS)

Journal of Information Systems Engineering and Management
2026, 11(3s)
e-ISSN: 2468-4376
https://www.jisem-journal.com/

Research Article

Figure 06 illustrates the effect of varying buffer layer thicknesses from 0.02 µm to 0.04 µm on the photovoltaic parameters (Voc, Jsc, FF and PCE). The results confirmed that variation in buffer layer thickness had a negligible impact on these parameters. As the buffer layer thickness increases, the low diffusion length of minority carriers leads to a higher recombination rate, which in turn reduces efficiency with 0.5 %. Based on the simulation, the optimal buffer layer thickness was determined to be 0.02 µm. The maximum efficiency achieved with CdS buffer layer was 21.41 %. The negligible variation in photovoltaic parameters observed with changes in buffer layer thickness can be also attributed to several factors. Firstly, the buffer layer may not be the limiting factor in the device performance, especially if its initial thickness (0.04 µm) is within the optimal range. Additionally, wide-bandgap material such as CdS exhibit high transparency, resulting in minimal photon absorption and negligible impact on the short-circuit current density Jsc with thickness variation [36]. Furthermore, highly conductive buffer layers introduce low series resistance, thereby maintaining stable open-circuit voltage (Voc) and fill factor (FF) across different thicknesses.

Moreover, the variation of thickness of window layer can affect the quantum efficiency QE. A clear decline in QE was observed near to infrared region as the buffer layer thickness increases. As the figure is shown, the optimized thickness (0.02 µm) ensures that the layer CdS captures and transmits these photons effectively to balance light absorption, carrier transport and recombination. The graph demonstrates that thinner CdS layers, particularly around 0.02 µm to 0.04 µm, allow for higher QE, whereas thicker layers, such as 0.10 µm, result in a reduction in QE. This trend is especially noticeable in the short-wavelength region (300-500 nm), as highlighted in the zoomed-in section. Also, the curve J-V got better shape for thinner layers of CdS the increasing in thickness of buffer layer can influence negatively on J-V curve. We can observe that the increasing in thickness of this layer leads to small shifting in curve as it was illustrated in the zoomed-in section. The computational study determinates the ideal thickness for this layer that was 0.02 µm.

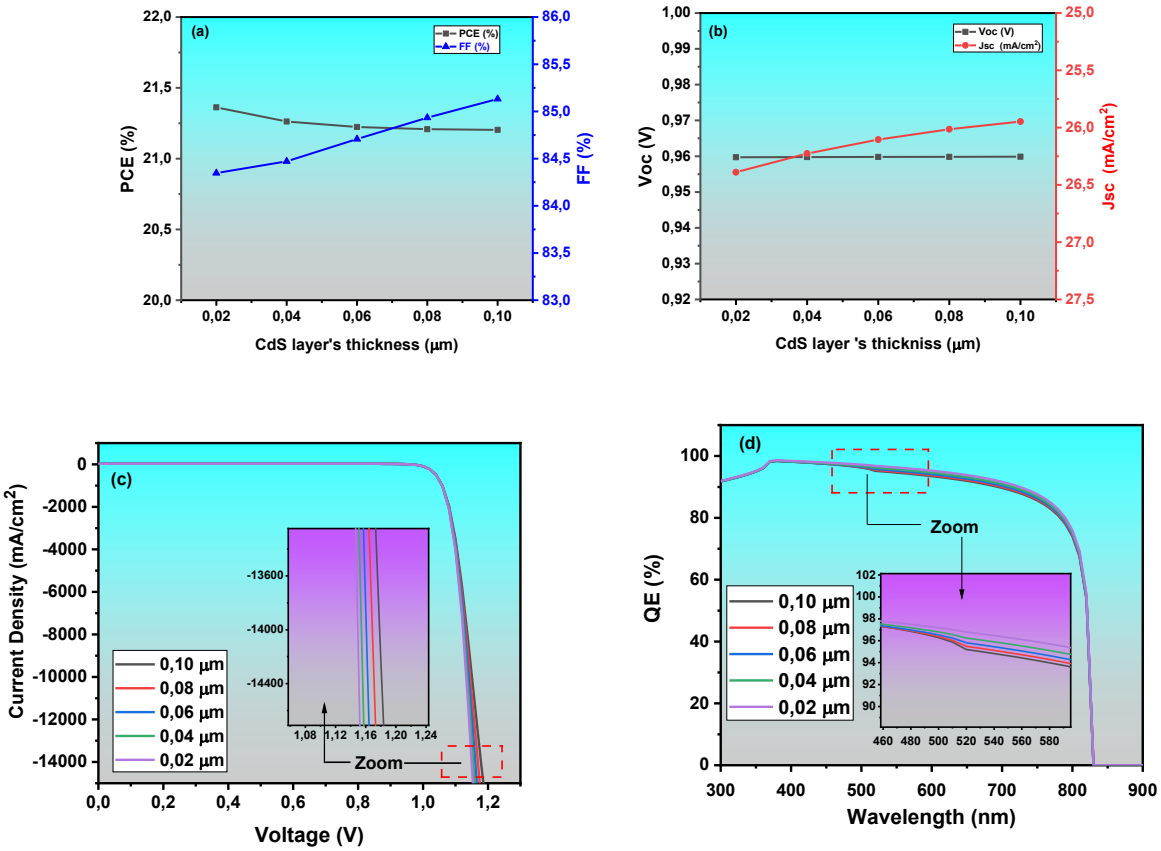

Figure 06. (a) and (b) Variations of Voc, Jsc, PCE and FF versus CdS's thickness. (c) and (d) variation of (J-V) and (QE) curves with increasing of thickness.

Journal of Information Systems Engineering and Management
2026, 11(3s)
e-ISSN: 2468-4376
https://www.jisem-journal.com/

Research Article

Thickness effect of window layer (Zn_2SnO_4)

The thickness of window layer Zn_2SnO_4 in solar cell plays critical role in enhancing its performances. In this step, the thickness of this layer Zn_2SnO_4 has been studied for different thickness ranging from 0.02 µm to 0.1 µm. The figure 07 confirmed that variation in window layer thickness had a negligible impact. more the thickness increases more the transparency of this layer Zn_2SnO_4 decreases leading to high absorption of light in this layer and decreasing the rate of absorption and generation pairs in absorber layer [37]. The increasing on thickness of Zn_2SnO_4 layer can lead to increase the absorption coefficient and reflection rate of the sun light of Zn_2SnO_4 layer due to the interference effect [38]. In addition, the decrease in QE with increasing thickness (in UV region) suggested that a thicker Zn_2SnO_4 layer introduced optical and electrical losses, negatively impacting the solar cell's overall performance. One possible reason for this decline is higher optical losses, where a thicker window layer absorbed or reflected more incoming photons before they reach the absorber layer, thereby reducing the number of generated charge carriers. These factors collectively contribute to the observed drop in QE with increasing Zn_2SnO_4 layer thickness, emphasizing the importance of optimizing thickness to balance light transmission and charge collection for improved solar cell efficiency [33]. Also, it was observed that the increasing in thickness of this layer could not affect J-V curves as it was illustrated in the zoomed-in section. The computational study determinates the ideal thickness for this layer that was 0.02 µm.

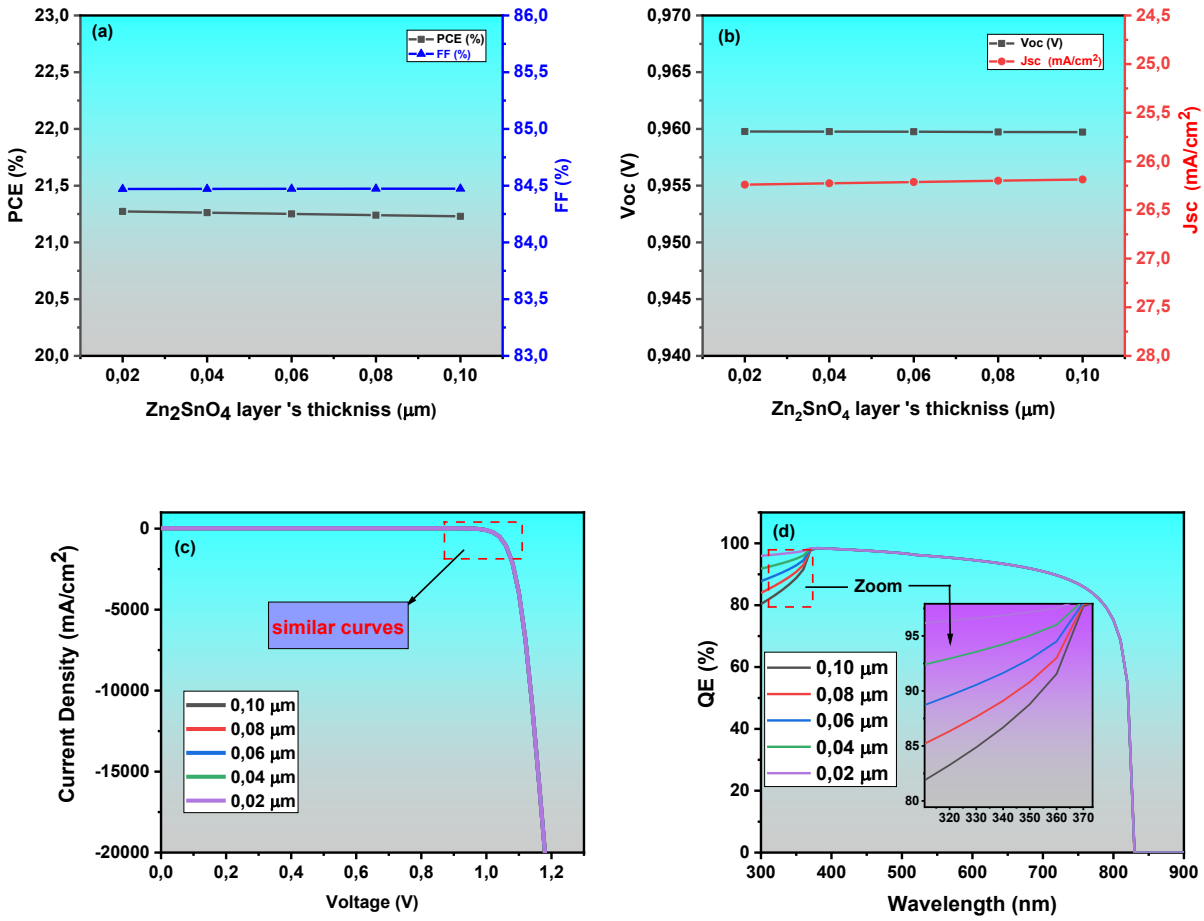

Figure 07. (a) and (b) Variations of Voc, Jsc, PCE and FF versus Zn_2SnO_4's thickness. (c) and (d) variation of (J-V) and (QE) curves with increasing of thickness.

Density defects effect in CuO layer

Journal of Information Systems Engineering and Management
2026, 11(3s)
e-ISSN: 2468-4376
https://www.jisem-journal.com/

Research Article

In this subsection, the photovoltaic parameters were investigated with different defects density (N_t) ranging from 10^{12} to 10^{18} cm^{-3}. According to figure 08, it is clear that the defects density negatively affected the performance of our solar cell and its photovoltaic parameters. The Voc decreased significantly from 0.96 to 0.88 V and the Jsc also decreased from 26.23 to 18.08 mA/cm^2. This behavior can be explained by several reasons. First, the increase in recombination centers and trapping electrons in grain boundaries [39, 40] which is described by Einstein's equation Eq. (12) [41]:

$$D = \mu \frac{K_B T}{q} \quad (12)$$

Where, D is the diffusion coefficient, μ is the carrier mobility, K_B is Boltazman constant, T is temperature and q is the elementary charge. Second, the decreasing of length diffusion and lifetime of pairs electron and hole (é/h). Furthermore, the J-V characteristic became distorted with the increasing of N_t consequently, the PCE and FF were decreased to 10.45 and 65.45 % respectively. Our findings are in good agreements with [3]. Moreover, the increase in defects density had a noticeable impact on the quantum efficiency (QE). As N_t increased, the QE spectrum exhibits a reduction across the both short and long wavelength which can attributed to the enhanced non-radiative recombination within the CuO layer and at the interfaces $CuO/CdS/Zn_2SnO_4$.

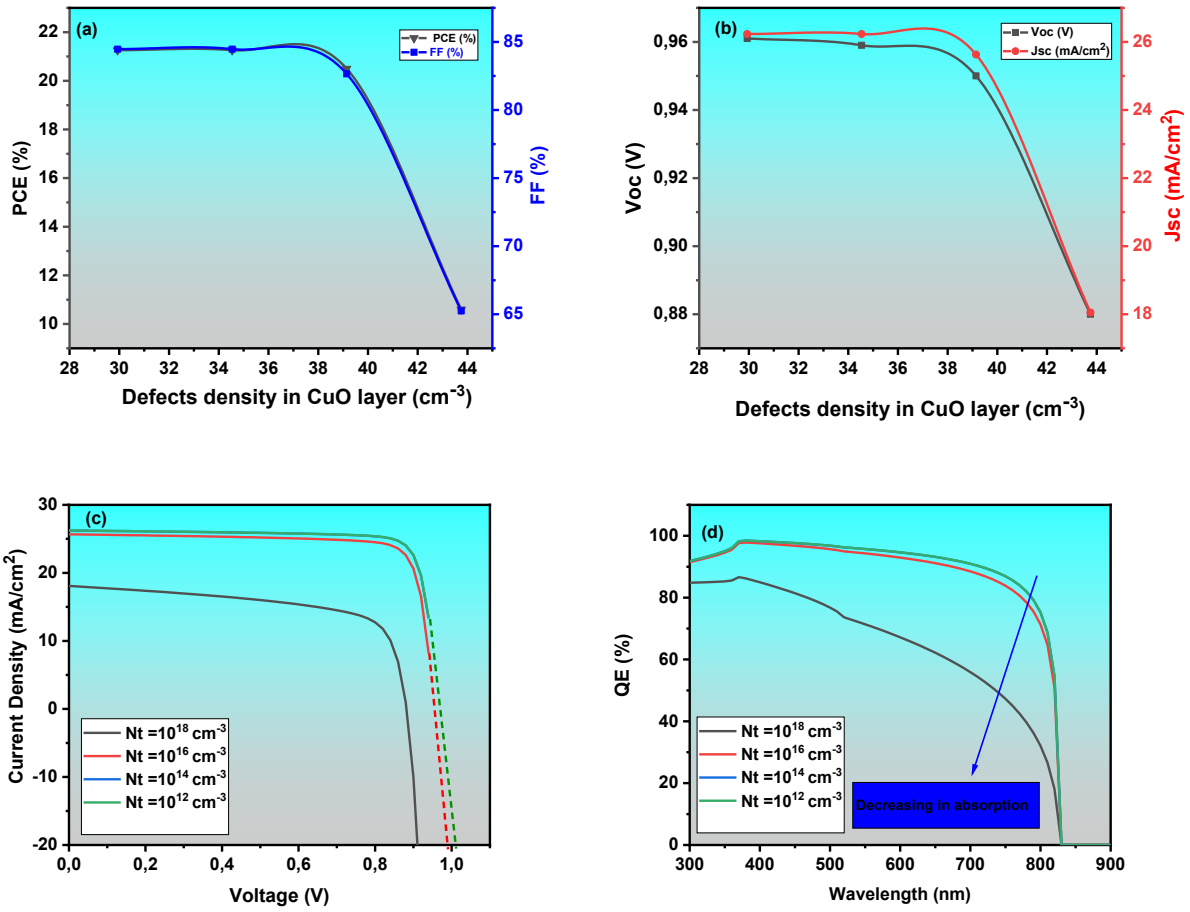

Figure 08. (a) and (b) Variations of Voc, Jsc, PCE and FF versus defects density, (c) and (d) variation of (J-V) and (QE) curves with increasing of defects density.

Work metal function effect

The nature of the back contact strongly influences the electronic and optical performance of p-type CuO-based thin-film solar cells. The simulations were performed using niobium (Nb, φ =4.9 eV), gold (Au, φ =5.1 eV), nickel (Ni,

Journal of Information Systems Engineering and Management
2026, 11(3s)
e-ISSN: 2468-4376
https://www.jisem-journal.com/

Research Article

φ =5.5 eV) and platinum (Pt, φ =5.7 eV). The parameters of Work metal function (MWF) for the contact materials used for the simulation are all based on the literature [15]. The figure 10 showed that the effect of MWF on the efficiency. For higher MWF values, the majority carrier barrier height decreased, indicating that the contact becomes more ohmic. Thus, as the work function of the metal increases, the Voc and efficiency also increase. This result is in good agreement with the data obtained by Anwar et al. [31]. In other word, metals such as Pt and Ni tend to form near-ohmic contacts, reducing interface recombination and preserving open-circuit voltage (Voc) and fill factor (FF). This trend was observed clearly with Pt (φ =5.7 eV), where the highest efficiency (PCE=28.60 %) was obtained with this metal, back contact engineering also affects photocurrent. Reflective metals may increase Jsc (28.73 mA/cm2) by acting as optical mirrors. On other hand, metals with lower work function, such as Nb (φ =4.9 eV) can form Schottky barriers (figure 09), which increase recombination, reduce Voc, and decrease FF. these findings are in good agreement with [8, 42, 43].

Our simulations typically involve sweeping back-contact work function, interface recombination velocity, and contact resistivity to explore how these factors influence device performance. Such analysis helps identify optimized back-contact stacks for high-efficiency, stable CuO absorber devices.

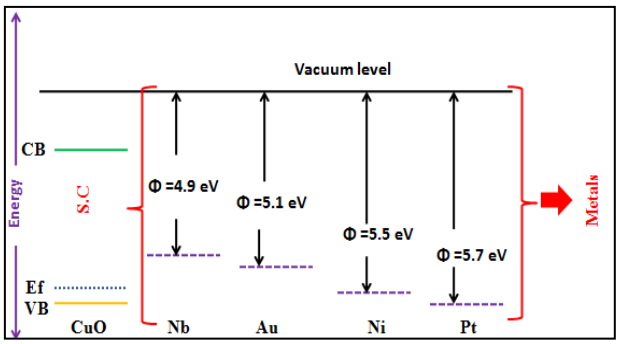

Figure 09. Illustration of energy levels for different metals.

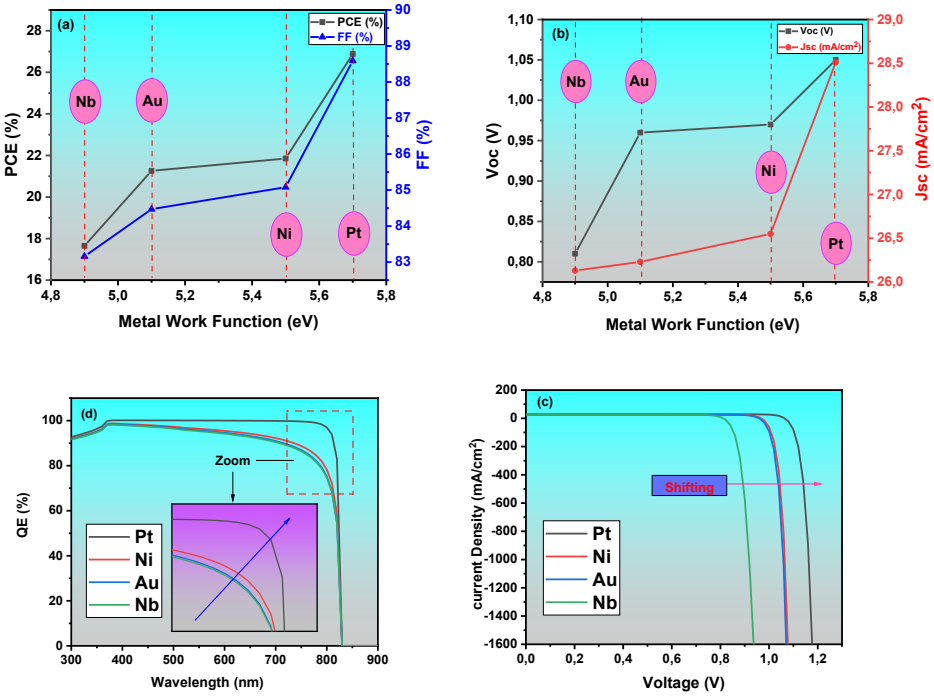

Figure 10. (a) and (b) Variations of Voc, Jsc, PCE and FF versus metal work function. (c) and (d) variation of (J-V) and (QE) curves with increasing of metal work function.

Journal of Information Systems Engineering and Management
2026, 11(3s)
e-ISSN: 2468-4376
https://www.jisem-journal.com/

Research Article

Resistance series and resistance shunt effect

The contour plots in Figure 11 provided a detailed and quantitative analysis of how the series resistance R_s and shunt resistance R_{sh} jointly determine the electronic behavior and overall efficiency of the simulated solar cell [33]. The influence of R_s arises from the ohmic voltage drop that reduces the actual voltage across the junction according to equation. Shunt resistance introduces a fundamentally different mechanism because R_{sh} modifies the leakage current that bypasses the diode [28]. The combined R_s-R_{sh} landscape reveals a clear synergy between these resistive elements. Low R_s alone is insufficient if R_{sh} is low, since leakage losses will dominate and suppress both Voc and Jsc [44]. Likewise, high Rsh alone cannot compensate for large R_s, because ohmic losses will still degrade FF and reduce output power. The contour maps indicate that the optimal performance domain occurs when Rs remains in the range of 2-4 Ω·cm² and R_{sh} exceeds approximately 10000 Ω·cm². In this region, the solar cell approaches its maximal theoreti cal limits, with high Voc, nearly ideal Jsc retention, an FF exceeding 70 %, and a peak efficiency above 19 %. Outside this optimal window, either excessive series resistance or insufficient shunt resistance becomes the dominant limiting mechanism. These results clearly demonstrate that achieving high-performance solar cells requires simultaneous optimization of contact quality and junction integrity by minimizing R_s and maximizing R_{sh} respectively, as the two parameters jointly dictate the curvature of the J-V curve and the position of the maximum power point [37].

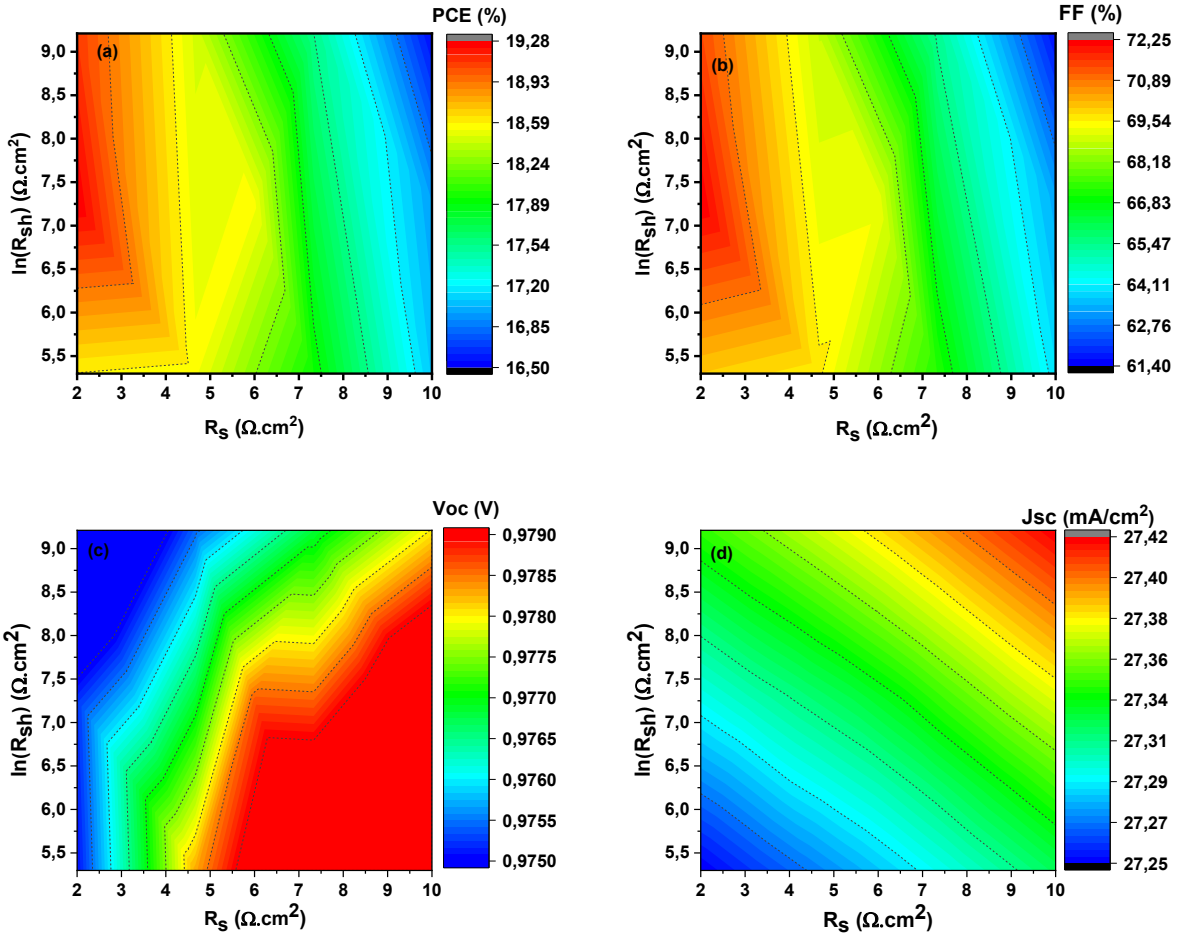

Figure 11. (a), (b), (c) and (d) mapping for Voc, Jsc, PCE and FF variation versus Rs/Rsh.

Acceptor concentration effect in CuO layer

In this part, the photovoltaic parameters were evaluated with different doping levels starting from 10^{16} to 10^{20} cm^{-3} of N_a in CuO layer in order to determine the optimized value of acceptor concentration in absorber layer. The figure 12 showed that the increasing in N_a can lead to an enhancement in the photovoltaic parameters, the PCE, FF and Voc

Journal of Information Systems Engineering and Management
2026, 11(3s)
e-ISSN: 2468-4376
https://www.jisem-journal.com/

Research Article

increased to 24.61 %, 88.90 % and 1.13 V at 10^{20} cm^{-3} respectively. Which can be explained by the reduction in series resistance and increasing of hole conductivity in CuO layer [45, 46]. However, the Jsc decreased to 25.23 mA/cm^2 as the acceptor concentration increased to 10^{20} cm^{-3}. These behaviors can be attributed to several mechanisms. First, the increasing in doping levels can lead to reduce the depletion width [3] which weakened the electrical field responsible for charge separation and collect ion, consequently, the mobility of carriers' chares decreased. Second, in heavy doped semiconductors, like CuO, they will act as metal material. In other words, the electronic orbitals associated with each acceptor impurity and the distance between impurities became so small. Finally, the increase of N_a in CuO layer can elevate recombination process because the electrons became very close to its holes [5]. Rahal et al. [4]. and Ranjan et al. [3] reported this correlation between the acceptor concentration and the photovoltaic parameters in their works about SCAPS study on the effect of various hole transport layer on highly efficient 31.86% eco-friendly CZTS based solar cell.

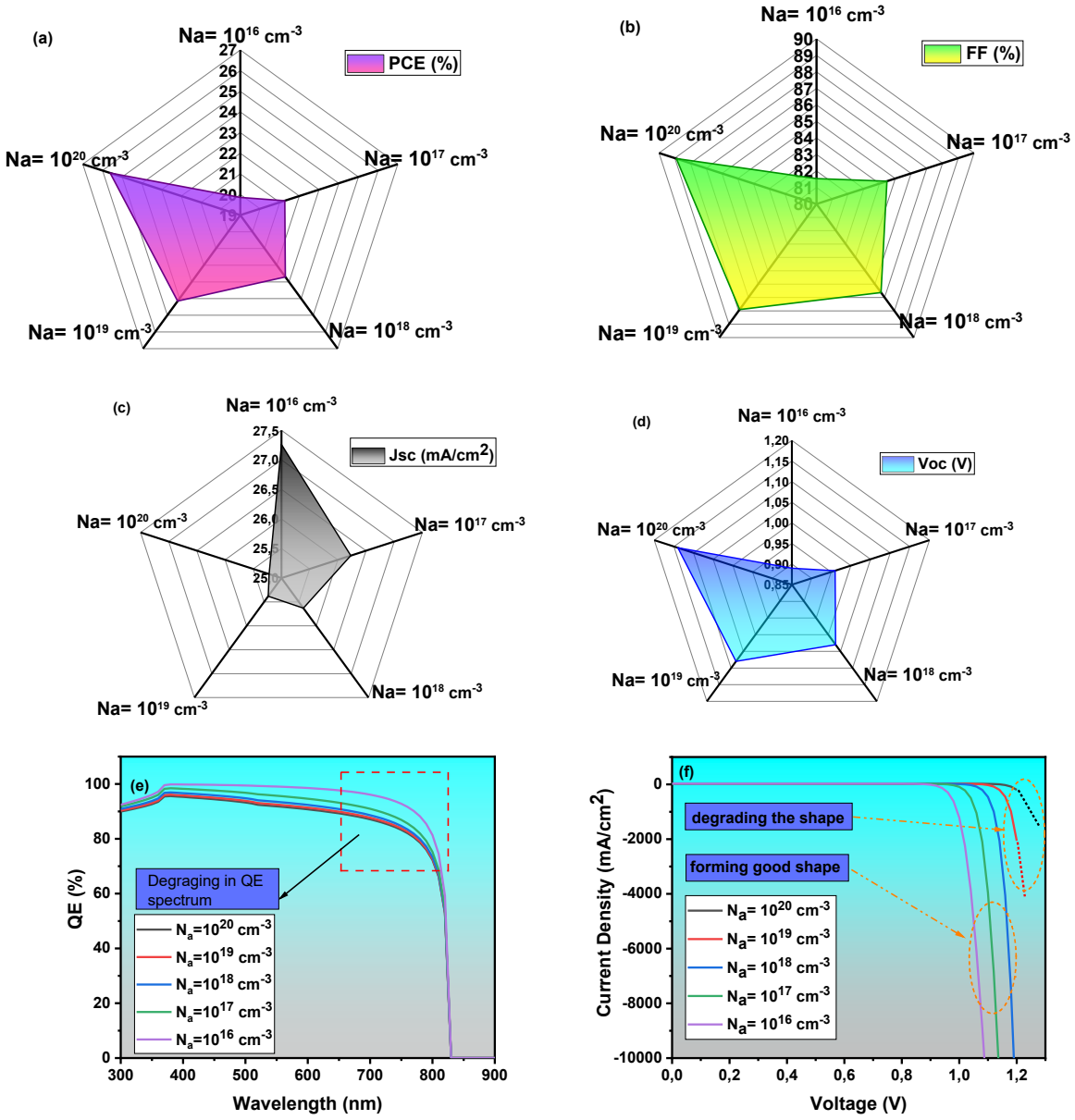

Figure 12. (a) ,(b) ,(c) and (d) mapping for Voc, Jsc, PCE and FF variation versus acceptor concentration. (e) and (f) variation of (J-V) and (QE) curves with increasing of acceptor concentration.

Journal of Information Systems Engineering and Management
2026, 11(3s)
e-ISSN: 2468-4376
https://www.jisem-journal.com/

Research Article

Optimized solar cell

Table 02 summarizes previously reported studies on CuO-based solar cells structure and compares them with the optimized Pt/CuO/CdS/Zn_2SnO_4 configuration obtained in this work. It is evident that the Pt/CuO/CdS/Zn_2SnO_4 structure, developed in the present study, is a strong candidate for solar panel fabrication. The optimized structure achieves an efficiency of 28.50% while using a relatively thin absorber layer, making it a promising option for sustainable and cost-effective solar cell production. The figure 12 showed J-V and QE curves for the optimized for cell. It is clear the J-V curve has better and high-quality shape reflected by high Voc an FF. In addition, the QE curve showed elevated absorption rate and high respond to light especially in visible range between 400 nm and 800 nm, which made our heterojunction Pt/CuO/CdS/Zn_2SnO_4 generate important PCE and Jsc.

Table 02. Comparative table with the previous studies.

Structure	Year	PCE (%)	FF (%)	Voc (V)	Jsc (mA/cm²)	References
Pt/CuO/CdS/Zn_2SnO_4	2026	28.50	89.11	1.12	28.73	Present work
CuO/ZrS_2	2023	23.8	72.2	0.96	34.2	[1]
CuO/TiO_2	2021	22.5	87.3	0.907	28.4	[15]
Sm-doped CuO/F:SnO_2	2025	15.98	86	0.72	30	[47]
Ag/CuO/ZnO/AZO/ITO	2021	8.92	82	0.73	14.80	[7]
CuO/$CH_3NH_3SnI_3$/SnO_2/FTO	2022	19.15	82.76	0.74	31.33	[48]
CuO/CdTe/CdS/TiO_2	2021	28.11	87.27	0.949	28.48	[49]

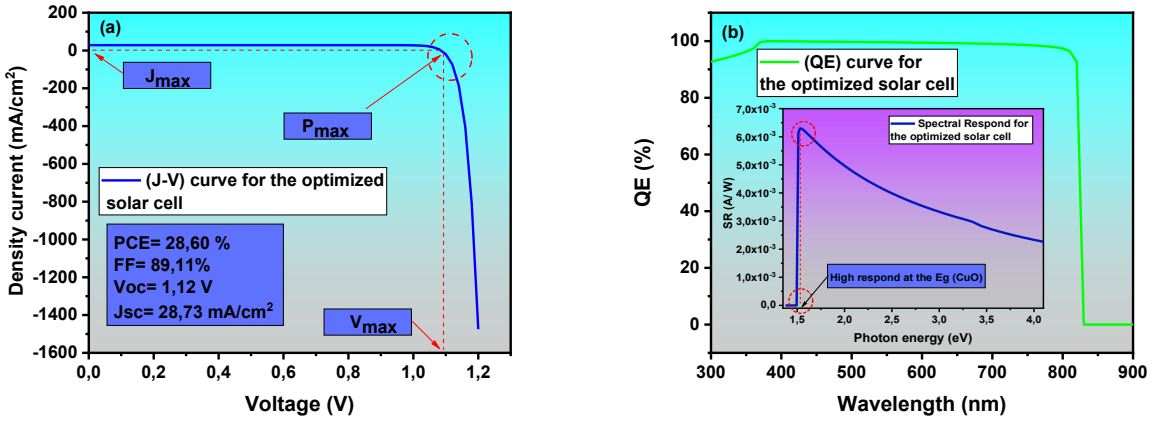

Figure 13. The (J-V) and (QE) curves for the optimized solar cell.

CONCLUSION

The simulation of CuO-based thin-films solar cells using SCAPS-1D has provided critical insights into the optimization of environmentally friendly and efficient photovoltaic structures. The analysis of absorber, buffer, and window layer thicknesses demonstrated that the CuO absorber layer plays the dominant role in determining performance, with an optimal thickness of 4 µm. In contrast, variations in buffer and window layer thicknesses produced only minor effects once their thicknesses exceeded the optical transmission threshold. Temperature dependent studies confirmed the expected decline in photovoltaic parameters with rising temperature, linked to increased carrier recombination and bandgap reduction. The optimized p-CuO/n-CdS/n-Zn_2SnO_4 configuration achieved an impressive efficiency of 28.50 % while using a thin absorber layer, confirming that high performance can be achieved with minimal material usage. These results suggest that CuO-based solar cells, when combined with Zn_2SnO_4 window layers, represent a promising pathway toward low-cost, non-toxic, and scalable thin-film photovoltaic devices. Future work should focus on experimental validation, interface defect reduction, and stability analysis under real operating conditions to further enhance device reliability and performance.

Journal of Information Systems Engineering and Management
2026, 11(3s)
e-ISSN: 2468-4376
https://www.jisem-journal.com/

Research Article

REFRENCES

[1] M. Abdelfatah, A. M. El Sayed, W. Ismail, S. Ulrich, V. Sittinger, and A. El-Shaer, "SCAPS simulation of novel inorganic ZrS2/CuO heterojunction solar cells," Sci. Rep., vol. 13, no. 1, Dec. 2023, doi: 10.1038/s41598-023-31553-4.

[2] E. A. Nyiekaa, T. A. Aika, E. Danladi, C. E. Akhabue, and P. E. Orukpe, "Simulation and optimization of 30.17% high performance N-type TCO-free inverted perovskite solar cell using inorganic transport materials," Sci. Rep., vol. 14, no. 1, Dec. 2024, doi: 10.1038/s41598-024-62882-7.

[3] R. Ranjan et al., "SCAPS study on the effect of various hole transport layer on highly efficient 31.86% eco-friendly CZTS based solar cell," Sci. Rep., vol. 13, no. 1, Dec. 2023, doi: 10.1038/s41598-023-44845-6.

[4] A. Rahal et al., "Optimization of structural and electronic properties in CuO/CIGS hybrid solar cells for high-efficiency, sustainable energy conversion," RSC Adv., vol. 15, no. 29, pp. 23311–23318, Jul. 2025, doi: 10.1039/d5ra04283f.

[5] M. U. Salman et al., "Direct correlation between open-circuit voltage and quasi-fermi level splitting in perovskite solar cells: a computational step involving thickness, doping, lifetime, and temperature variations for green solutions," RSC Adv., vol. 15, no. 20, pp. 15618–15629, May 2025, doi: 10.1039/d5ra01868d.

[6] S. H. Zyoud et al., "Numerical modeling of high conversion efficiency fto/zno/cds/czts/mo thin film-based solar cells: Using scaps-1d software," Crystals (Basel)., vol. 11, no. 12, Dec. 2021, doi: 10.3390/cryst11121468.

[7] J. Husna, P. S. Menon, P. Chelvanathan, M. A. Mohamed, S. K. Tripathy, and T. R. Lenka, "Numerical study of semi-transparent thin film heterojunction p-CuO/nZnO/AZO/ITO solar cells device model using SCAPS-1D," Chalcogenide Letters, vol. 18, no. 11, pp. 667–679, Nov. 2021, doi: 10.15251/CL.2021.1811.667.

[8] L. A. Lotfy, M. Abdelfatah, S. W. Sharshir, A. A. El-Naggar, W. Ismail, and A. El-Shaer, "Numerical simulation and optimization of FTO/TiO2/CZTS/CuO/Au solar cell using SCAPS-1D," Sci. Rep., vol. 15, no. 1, Dec. 2025, doi: 10.1038/s41598-025-12999-0.

[9] M. A. Salih, M. A. Mustafa, and B. A. A. Yousef, "Developing Lead-Free Perovskite-Based Solar Cells with Planar Structure in Confined Mode Arrangement Using SCAPS-1D," Sustainability (Switzerland), vol. 15, no. 2, Jan. 2023, doi: 10.3390/su15021607.

[10] M. R. Kabir et al., "A comprehensive SCAPS-1D simulation study on the photovoltaic properties and efficiency enhancement of CH3NH3PbCl3 perovskite solar cells," Engineering Research Express, vol. 7, no. 1, Mar. 2025, doi: 10.1088/2631-8695/ada721.

[11] A. Kaphle, E. Echeverria, D. N. McLlroy, and P. Hari, "Enhancement in the performance of nanostructured CuO-ZnO solar cells by band alignment," RSC Adv., vol. 10, no. 13, pp. 7839–7854, Feb. 2020, doi: 10.1039/c9ra10771a.

[12] K. Sarker, M. S. Sumon, M. F. Orthe, S. K. Biswas, and M. M. Ahmed, "Numerical Simulation of High Efficiency Environment Friendly CuBi2O4-Based Thin-Film Solar Cell Using SCAPS-1D," International Journal of Photoenergy, vol. 2023, 2023, doi: 10.1155/2023/7208502.

[13] Md. S. Reza et al., " High-efficiency and eco-friendly Cs 2 SnBr 6 -based perovskite solar cells: optimized device architecture and performance analysis via SCAPS-1D simulation ," Opt. Express, vol. 33, no. 14, p. 30441, Jul. 2025, doi: 10.1364/oe.566116.

[14] M. A. Rahman, "Design and simulation of a high-performance Cd-free Cu2SnSe3 solar cells with SnS electron-blocking hole transport layer and TiO2 electron transport layer by SCAPS-1D," SN Appl. Sci., vol. 3, no. 2, Feb. 2021, doi: 10.1007/s42452-021-04267-3.

[15] P. Sawicka-Chudy et al., "Simulation of TiO2/CuO solar cells with SCAPS-1D software," Mater. Res. Express, vol. 6, no. 8, Jun. 2019, doi: 10.1088/2053-1591/ab22aa.

[16] M. A. Rahman, "Design and simulation of a high-performance Cd-free Cu2SnSe3 solar cells with SnS electron-blocking hole transport layer and TiO2 electron transport layer by SCAPS-1D," SN Appl. Sci., vol. 3, no. 2, Feb. 2021, doi: 10.1007/s42452-021-04267-3.

[17] M. A. Ghebouli, B. Ghebouli, R. Larbi, T. Chihi, and M. Fatmi, "Effect of buffer nature, absorber layer thickness and temperature on the performance of CISSe based solar cells, using SCAPS-1D simulation program," Optik (Stuttg)., vol. 241, Sep. 2021, doi: 10.1016/j.ijleo.2020.166203.

[18] A. P. Shyma and R. Sellappan, "Computational Probing of Tin-Based Lead-Free Perovskite Solar Cells: Effects of Absorber Parameters and Various Electron Transport Layer Materials on Device Performance," Materials, vol. 15, no. 21, Nov. 2022, doi: 10.3390/ma15217859.
[19] S. Mehmood, Y. Xia, F. Qu, and M. He, "Investigating the Performance of Efficient and Stable Planer Perovskite Solar Cell with an Effective Inorganic Carrier Transport Layer Using SCAPS-1D Simulation," Energies (Basel)., vol. 16, no. 21, Nov. 2023, doi: 10.3390/en16217438.
[20] J. Al Mahmud et al., "Design and analysis of a SnS2/WS2/V2O5 double-heterojunction toward high-performance photovoltaics," Energy Advances, vol. 2, no. 11, pp. 1843–1858, Sep. 2023, doi: 10.1039/d3ya00231d.
[21] R. M. Moinuddin, M. Hasan, M. Rahaman, and K. S. Islam, "Numerical optimization and efficiency analysis of Sn-based perovskite-on-silicon tandem solar cells with various TCO materials using SCAPS-1D simulation," AIP Adv., vol. 14, no. 8, Aug. 2024, doi: 10.1063/5.0217477.
[22] A. Yousfi et al., "Design and simulation of high efficiency KSnI3 based perovskite solar cells using DFT and SCAPS-1D," Sci. Rep., vol. 15, no. 1, Dec. 2025, doi: 10.1038/s41598-025-19579-2.
[23] A. Shaikh, P. Hameed Shaikh, S. Ahmed Khatri, M. Saeed, H. Shah, and L. Kumar, "Performance Optimization in Lead-Free Perovskite Solar Cell: A Comparative Approach," IEEE Access, vol. 13, pp. 40747–40759, 2025, doi: 10.1109/ACCESS.2025.3543244.
[24] M. K. Mim and S. K. Biswas, "Performance Analysis of Sr3SbI3-Based Perovskite Solar Cell Using SCAPS-1D Software," Advances in Materials Science and Engineering, vol. 2025, no. 1, 2025, doi: 10.1155/amse/7134012.
[25] R. A. Rassol, R. F. Hasan, and S. M. Ahmed, "Numerical analysis of SnO2/Zn2SnO4/n-CdS/p-CdTe solar cell using the SCAPS-1D simulation software," Iraqi Journal of Science, vol. 62, no. 2, pp. 505–516, Feb. 2021, doi: 10.24996/ijs.2021.62.2.17.
[26] M. Noman, A. H. H. Khan, and S. T. Jan, "Interface engineering and defect passivation for enhanced hole extraction, ion migration, and optimal charge dynamics in both lead-based and lead-free perovskite solar cells," Sci. Rep., vol. 14, no. 1, Dec. 2024, doi: 10.1038/s41598-024-56246-4.
[27] J. C. Z. Medina et al., "Numerical Simulation and Performance Optimization of a Solar Cell Based on WO3/CdTe Heterostructure Using NiO as HTL Layer by SCAPS 1D," Coatings, vol. 13, no. 8, Aug. 2023, doi: 10.3390/coatings13081436.
[28] H. Heriche, Z. Rouabah, and N. Bouarissa, "New ultra thin CIGS structure solar cells using SCAPS simulation program," Int. J. Hydrogen Energy, vol. 42, no. 15, pp. 9524–9532, Apr. 2017, doi: 10.1016/j.ijhydene.2017.02.099.
[29] B. V. Kheswa and S. N. T. Majola, "Simulation of novel CsSnBr3 perovskite solar cells achieving efficiency of 31.62 %," Phys. Scr., vol. 100, no. 1, Jan. 2025, doi: 10.1088/1402-4896/ad986e.
[30] A. C. Ozurumba et al., "SCAPS-1D simulated organometallic halide perovskites: A comparison of performance under Sub-Saharan temperature condition," Heliyon, vol. 10, no. 8, Apr. 2024, doi: 10.1016/j.heliyon.2024.e29599.
[31] T. Titu, "Simulation Study of Cs 2 TiBr 6 Perovskite Solar Cells Using Graphene Oxide as a Novel HTL Layer Using SCAPS 1-D," vol. 4, no. 2, pp. 159–169, 2023, doi: 10.22044/rera.2022.12175.1154.
[32] S. Bhandari, A. Roy, A. Ghosh, T. K. Mallick, and S. Sundaram, "Perceiving the temperature coefficients of carbon-based perovskite solar cells," Sustain. Energy Fuels, vol. 4, no. 12, pp. 6283–6298, Dec. 2020, doi: 10.1039/d0se00782j.
[33] E. A. Nyiekaa, T. A. Aika, E. Danladi, C. E. Akhabue, and P. E. Orukpe, "Simulation and optimization of 30.17% high performance N-type TCO-free inverted perovskite solar cell using inorganic transport materials," Sci. Rep., vol. 14, no. 1, Dec. 2024, doi: 10.1038/s41598-024-62882-7.
[34] T. A. Chowdhury, "Simulation Study of CuO-Based Solar Cell with Different Buffer Layers Using SCAPS-1D," Energy Power Eng., vol. 15, no. 09, pp. 307–314, 2023, doi: 10.4236/epe.2023.159016.
[35] M. K. Hossain et al., "Deep Insights into the Coupled Optoelectronic and Photovoltaic Analysis of Lead-Free CsSnI3 Perovskite-Based Solar Cell Using DFT Calculations and SCAPS-1D Simulations," ACS Omega, vol. 8, no. 25, pp. 22466–22485, Jun. 2023, doi: 10.1021/acsomega.3c00306.

[36] A. A. El-Naggar et al., "SCAPS simulation and design of highly efficient CuBi2O4-based thin-film solar cells (TFSCs) with hole and electron transport layers," Sci. Rep., vol. 15, no. 1, Dec. 2025, doi: 10.1038/s41598-025-12091-7.
[37] Naureen, Sadanand, S. Rai, R. K. Yadav, P. Lohia, and Prof. D. K. Dwivedi, "A Simulation Study of Quantum Dot Solar Cells Using Two Distinct ETL of WO3 and WS2," Jul. 12, 2022. doi: 10.21203/rs.3.rs-1808284/v1.
[38] A. Shrivastava, S. Saini, D. Kumari, S. Singh, and J. Adam, "Quantum-to-classical modeling of monolayer Ge2Se2 and its application in photovoltaic devices," Beilstein Journal of Nanotechnology, vol. 15, pp. 1153–1169, 2024, doi: 10.3762/BJNANO.15.94.
[39] P. Xu et al., "Grain Boundaries Contribute to the Performance of Perovskite Solar Cells by Promoting Charge Separations," Nanomicro Lett., vol. 17, no. 1, Dec. 2025, doi: 10.1007/s40820-025-01795-0.
[40] X. Li, Y. Fang, and J. Zhao, "Optimizing Inorganic Cs4CuSb2Cl12/Cs2TiI6 Dual-Absorber Solar Cells: SCAPS-1D Simulations and Machine Learning," Nanomaterials, vol. 15, no. 16, Aug. 2025, doi: 10.3390/nano15161245.
[41] H. Abboudi et al., "Optimization of InxGa1–xN P-I-N Solar Cells: Achieving 21% Efficiency Through SCAPS-1D Modeling," Crystals (Basel)., vol. 15, no. 7, Jul. 2025, doi: 10.3390/cryst15070633.
[42] M. Tarekuzzaman and K. I. F. Utsho, "Advancing Solar Energy with Cs2TlAsI6 Double Halide Perovskite: A Simulation-Driven Approach for High-Efficiency Solar Cell," Adv. Electron. Mater., vol. 11, no. 16, Oct. 2025, doi: 10.1002/aelm.202500312.
[43] H. J. Park, H. Son, and B. S. Jeong, "SCAPS-1D Simulation for Device Optimization to Improve Efficiency in Lead-Free CsSnI3 Perovskite Solar Cells," Inorganics (Basel)., vol. 12, no. 4, Apr. 2024, doi: 10.3390/inorganics12040123.
[44] A. Mortadi, E. El Hafidi, H. Nasrellah, M. Monkade, and R. El Moznine, "Analysis and optimization of lead-free perovskite solar cells: investigating performance and electrical characteristics," Mater. Renew. Sustain. Energy, vol. 13, no. 2, pp. 219–232, Aug. 2024, doi: 10.1007/s40243-024-00260-z.
[45] S. Upadhyay and D. Singh, "EFFECT OF SERIES AND SHUNT RESISTANCE ON THE PERFORMANCE OF KESTERITE SOLAR CELLS," International Journal of Scientific Research in Modern Science and Technology, vol. 2, no. 8, pp. 38–45, Aug. 2023, doi: 10.59828/ijsrmst.v2i8.134.
[46] Z. Younsi et al., "Scrutinizing transport phenomena and recombination mechanisms in thin film Sb2S3 solar cells," Sci. Rep., vol. 14, no. 1, Dec. 2024, doi: 10.1038/s41598-024-56041-1.
[47] G. Charrada et al., "Synthesis of Sm-Doped CuO–SnO2:FSprayed Thin Film: An Eco-Friendly Dual-Function Solution for the Buffer Layer and an Effective Photocatalyst for Ampicillin Degradation," Technologies (Basel)., vol. 13, no. 5, May 2025, doi: 10.3390/technologies13050197.
[48] C. I. Hussain, Y. M. Hassan, and F. A. Abed, "Optimization of Organic-Inorganic Perovskite Solar Cell Layers," Sep. 23, 2022. doi: 10.21203/rs.3.rs-2084341/v1.
[49] A. Roy and A. Majumdar, "Optimization of CuO/CdTe/CdS/TiO2 solar cell efficiency: A numerical simulation modeling," Optik (Stuttg)., vol. 251, Feb. 2022, doi: 10.1016/j.ijleo.2021.168456.